PLOS GENETICS

RESEARCH ARTICLE

Inhibition of FLT1 ameliorates muscular dystrophy phenotype by increased vasculature in a mouse model of Duchenne muscular dystrophy

Mayank Verma[1,2,3,4], Yuko Shimizu-Motohashi[2,3,4], Yoko Asakura[2,3,4], James P. Ennen[2,3,4], Jennifer Bosco[5], Zhiwei Zhou[5], Guo-Hua Fong[6], Serene Josiah[5], Dennis Keefe[5], Atsushi Asakura[2,3,4]*

1 Medical Scientist Training Program, University of Minnesota Medical School, Minneapolis, MN, United States of America, **2** Stem Cell Institute, University of Minnesota Medical School, Minneapolis, MN, United States of America, **3** Paul & Sheila Wellstone Muscular Dystrophy Center, University of Minnesota Medical School, Minneapolis, MN, United States of America, **4** Department of Neurology, University of Minnesota Medical School, Minneapolis, MN, United States of America, **5** Shire Human Genetic Therapies, Inc., a member of the Takeda group of companies, Lexington, MA, United States of America, **6** Center for Vascular Biology, University of Connecticut Health Center, University of Connecticut School of Medicine, Farmington, CT, United States of America

* asakura@umn.edu

Citation: Verma M, Shimizu-Motohashi Y, Asakura Y, Ennen JP, Bosco J, Zhou Z, et al. (2019) Inhibition of FLT1 ameliorates muscular dystrophy phenotype by increased vasculature in a mouse model of Duchenne muscular dystrophy. PLoS Genet 15(12): e1008468. https://doi.org/10.1371/journal.pgen.1008468

Editor: Gregory A. Cox, The Jackson Laboratory, UNITED STATES

Received: May 22, 2019

Accepted: October 8, 2019

Published: December 26, 2019

Data Availability Statement: All relevant data are within the manuscript and its Supporting Information files.

Funding: This work was supported by NIHT32-GM008244 and NIHF30-AR066454 to MV, and NIHR03-AR061545, MDA (MDA241600) and a grant from Shire Human Genetic Therapies Inc., a member of the Takeda group of companies to AA. The funders had no role in study design, data

Abstract

Duchenne muscular dystrophy (DMD) is an X-linked recessive genetic disease in which the dystrophin coding for a membrane stabilizing protein is mutated. Recently, the vasculature has also shown to be perturbed in DMD and DMD model *mdx* mice. Recent DMD transcriptomics revealed the defects were correlated to a vascular endothelial growth factor (VEGF) signaling pathway. To reveal the relationship between DMD and VEGF signaling, *mdx* mice were crossed with constitutive ($CAG^{CreERTM}$:$Flt1^{LoxP/LoxP}$) and endothelial cell-specific conditional gene knockout mice ($Cdh5^{CreERT2}$:$Flt1^{LoxP/LoxP}$) for *Flt1* (VEGFR1) which is a decoy receptor for VEGF. Here, we showed that while constitutive deletion of *Flt1* is detrimental to the skeletal muscle function, endothelial cell-specific *Flt1* deletion resulted in increased vascular density, increased satellite cell number and improvement in the DMD-associated phenotype in the *mdx* mice. These decreases in pathology, including improved muscle histology and function, were recapitulated in *mdx* mice given anti-FLT1 peptides or monoclonal antibodies, which blocked VEGF-FLT1 binding. The histological and functional improvement of dystrophic muscle by FLT1 blockade provides a novel pharmacological strategy for the potential treatment of DMD.

Author summary

Duchenne muscular dystrophy (DMD) is a devastating muscle disease affecting one in 5,000 newborn males, in which the gene encoding the dystrophin protein is mutated. It is a progressive muscle degenerative disease with death by either respiratory insufficiency or

collection and analysis, decision to publish, or preparation of the manuscript.

Competing interests: MV, AA, SJ and DK are listed as inventors on a patent for antibody mediated therapy for DMD. JB, ZZ, SJ and DK are employed by Shire Human Genetic Therapies, Inc., a member of the Takeda group of companies, and own shares/stock in the company. AA received a grant from Shire Human Genetic Therapies, Inc., a member of the Takeda group of companies, for antibody mediated therapy for DMD.

cardiac failure in their 20s. Recently, the vasculature has also shown to be perturbed in DMD and DMD model *mdx* mice with the defects correlated to a vascular endothelial growth factor (VEGF) signaling pathway. To reveal the relationship between DMD and VEGF signaling, *mdx* mice were crossed with mice carrying mutated a decoy receptor gene (*Flt1*) for VEGF. Here, we showed that *Flt1* deletion resulted in increased vascular density and improvement in the DMD-associated skeletal muscle phenotype in the *mdx* mice. These decreases in pathology, including improved muscle histology and function, were recapitulated in *mdx* mice given anti-FLT1 peptides or monoclonal antibodies, which blocked VEGF-FLT1 binding. The histological and functional improvement of dystrophic muscle by FLT1 blockade provides a novel pharmacological strategy for the potential treatment of DMD.

Introduction

Duchenne muscular dystrophy (DMD) is an X-linked muscle disease affecting one in 5,000 newborn males, in which the gene encoding the dystrophin protein is mutated. It is a progressive neurodegenerative disease with clinical symptoms manifesting at 2–3 years of age, loss of ambulation in early teen years and death by either respiratory insufficiency or cardiac failure in their 20s. A disease model for DMD is the *mdx* mouse, which lacks functional dystrophin expression due to a point mutation in the dystrophin gene. The *mdx* mouse has been extensively characterized and contributed to the understanding of the disease pathology [1].

Although the role of dystrophin in the skeletal muscle is widely appreciated, endothelium and vascular smooth muscle cells also express dystrophin [2]. The absence of dystrophin in these cells induced vessel dilation and abnormal blood flow, resulting in a state of functional ischemia, worsening the muscle pathology in *mdx* mice [3]. Restoration of dystrophin specifically in the smooth muscle of the vasculature rescued some aspects of the skeletal muscle pathology associated with the *mdx* mice [4]. Disruption of the dystrophin-associated sarcoglycan complex in vascular smooth muscle perturbed vascular function resulting in exacerbation of muscular dystrophic changes [5]. Dystrophin is responsible for anchoring neuronal nitric oxide synthase (nNOS) to the cell surface, which is crucial for exercise-induced increases in blood supply in muscle via NO-mediated vasodilation [6]. Administration of a phosphodiesterase-5 (PDE-5) inhibitors to *mdx* mice, which increased NO production, rescued the muscle from this state of functional ischemia, and improved muscle function in *mdx* mice [7, 8]. Similarly in humans, PDE-5 inhibitors given to both DMD boys and adult patients with Becker muscular dystrophy (BMD), a milder form of muscular dystrophy, alleviated functional ischemia during muscle contraction [9, 10]. More recent data showed that *mdx* skeletal muscle was less perfused and displayed marked microvessel alterations compared to wild-type C57BL6 mice [11, 12]. While current studies support the importance of NO-mediated vasodilation in DMD, the relationship between DMD and angiogenesis is not well understood.

Vascular endothelial growth factor (VEGF) signaling is one of the strongest modulators of angiogenesis and includes the ligands VEGFA, VEGFB, VEGFC and PlGF. VEGFA is the most well studied ligand of the system and acts through its two receptors, VEGF receptor-1 (VEGFR1/FLT1) and VEGF receptor-2 (VEGFR2/FLK1/KDR). Although FLK1 possesses stronger signaling capabilities, FLT1 has considerably higher affinity for VEGF but weaker signaling capabilities. In normal tissue, FLT1 acts as a sink trap for VEGF thereby preventing excessive pathological angiogenesis [13]. In addition, soluble FLT1 (sFLT1) functions as an endogenous VEGF trap [14]. Despite the known angiogenic defect in DMD and *mdx* mice, it is not known whether VEGF and its receptors are implicated in this disease process. Previous

data from our laboratory demonstrated that heterozygous *Flt1* gene knockout ($Flt1^{+/-}$) mice were viable and displayed developmentally increased capillary density in the skeletal muscles [15]. Importantly, when crossed $Flt1^{+/-}$ with *mdx* or *mdx*:$utrophin^{-/-}$ mice, these mice displayed both histological and functional improvements of the dystrophic pathologic phenotype. However, it remained unknown whether postnatal *Flt1* gene deletion could recapitulate these improvements in *mdx* mice. Since *Flt1* is detected in several cell types including endothelial cells, myeloid cells and some neurons [16–18], it is important to know which cell type is important for the beneficial effects of FLT1-associated improvements seen in the *mdx* mice. Lastly, it remained to be seen whether blockage of FLT1 could be exploited pharmacologically to recapitulate the muscle improvements seen in the genetic models.

In this report, we compared adult *mdx* mice with a constitutive conditional knockout and an endothelial cell-specific conditional knockout of *Flt1*. We showed that endothelial cell-specific *Flt1* deletion increased the capillary density in skeletal muscle and improved the DMD-associated muscle pathology. In addition, we showed that systemic delivery of anti-FLT1 peptides and monoclonal antibodies (MAbs) in *mdx* mice recapitulated the reduction in DMD-associated pathology seen after *Flt1* deletion in *mdx* mice, validating *Flt1* as a therapeutic target for the treatment of DMD.

Results

Postnatal *Flt1* gene deletion in mice displays increase in capillary density

We previously found that *mdx* mice developmentally lacking one copy of the *Flt1* allele have increased muscle angiogenesis and improved muscle pathology [14]. To investigate whether postnatal deletion of *Flt1* gene could affect the vasculature density, we crossed $CAG^{CreERTM}$ mice carrying a constitutively expressed $CreER^{TM}$ gene [19] with $Flt1^{LoxP/LoxP}$ mice [20] to generate conditional *Flt1* gene knockout ($CAG^{CreERTM}$:$Flt1^{LoxP/LoxP}$) mice (Fig 1A). Upon treatment with tamoxifen (TMX), which leads to global *Flt1* gene and FLT1 protein deletion (S1A and S1B Fig), $Flt1^{\Delta/\Delta}$ mice displayed significantly increased CD31+ vascular density compared to the $Flt1^{+/+}$ ($Flt1^{LoxP/LoxP}$) mice (Fig 1B and 1C). The increase in capillary density following TMX-mediated *Flt1* gene deletion was rapid (within 8 days) and long lasting (more than 207 days) (Fig 1D). This allowed us to be confident that we were able to phenotype late term changes following deletion of *Flt1* gene. Postnatal global loss of *Flt1* resulted in a reduction in body mass [21] without reduction of tibialis anterior (TA) muscle mass (S1C and S1D Fig).

mdx:$Flt1^{\Delta/\Delta}$ mice display worse muscle pathology compared to control *mdx*:$Flt1^{+/+}$ mice

As we did not see any gross changes in the skeletal muscle except for increased vascular density in the $Flt1^{\Delta/\Delta}$ mice, we crossed the *mdx* mice to the $CAG^{CreERTM}$:$Flt1^{LoxP/LoxP}$ to obtain *mdx*:$CAG^{CreERTM}$:$Flt1^{LoxP/LoxP}$ mice. We obtained these mice in expected mendelian ratios (S2A Fig). Our original goal was to induce *Flt1* gene deletion prior to the onset of muscle pathology, thus before postnatal day 21 (p21), by treatment with TMX or its active form, 4-hydroxy tamoxifen (4-OHT). However, perinatal loss of *Flt1* resulted in lethality when TMX or 4-OHT treatment was initiated at p3 or p5 and partial lethality at p16 in *mdx*:$CAG^{CreERTM}$:$Flt1^{LoxP/LoxP}$ (*mdx*:$Flt1^{\Delta/\Delta}$) mice (S2B Fig), indicating that *Flt1* is required in the perinatal stage for survival. The mice displayed no lethality when recombination was induced on or after p21. Similar to the $Flt1^{\Delta/\Delta}$ mice, body mass decreased without changing muscle mass in *mdx*:$Flt1^{\Delta/\Delta}$ mice compared with *mdx*:$Flt1^{+/+}$ mice (S2C and S2D Fig). The *mdx*:$Flt1^{\Delta/\Delta}$ mice displayed notable white fur, a sign of premature aging or stress (S3A Fig). Importantly, the increase in capillary

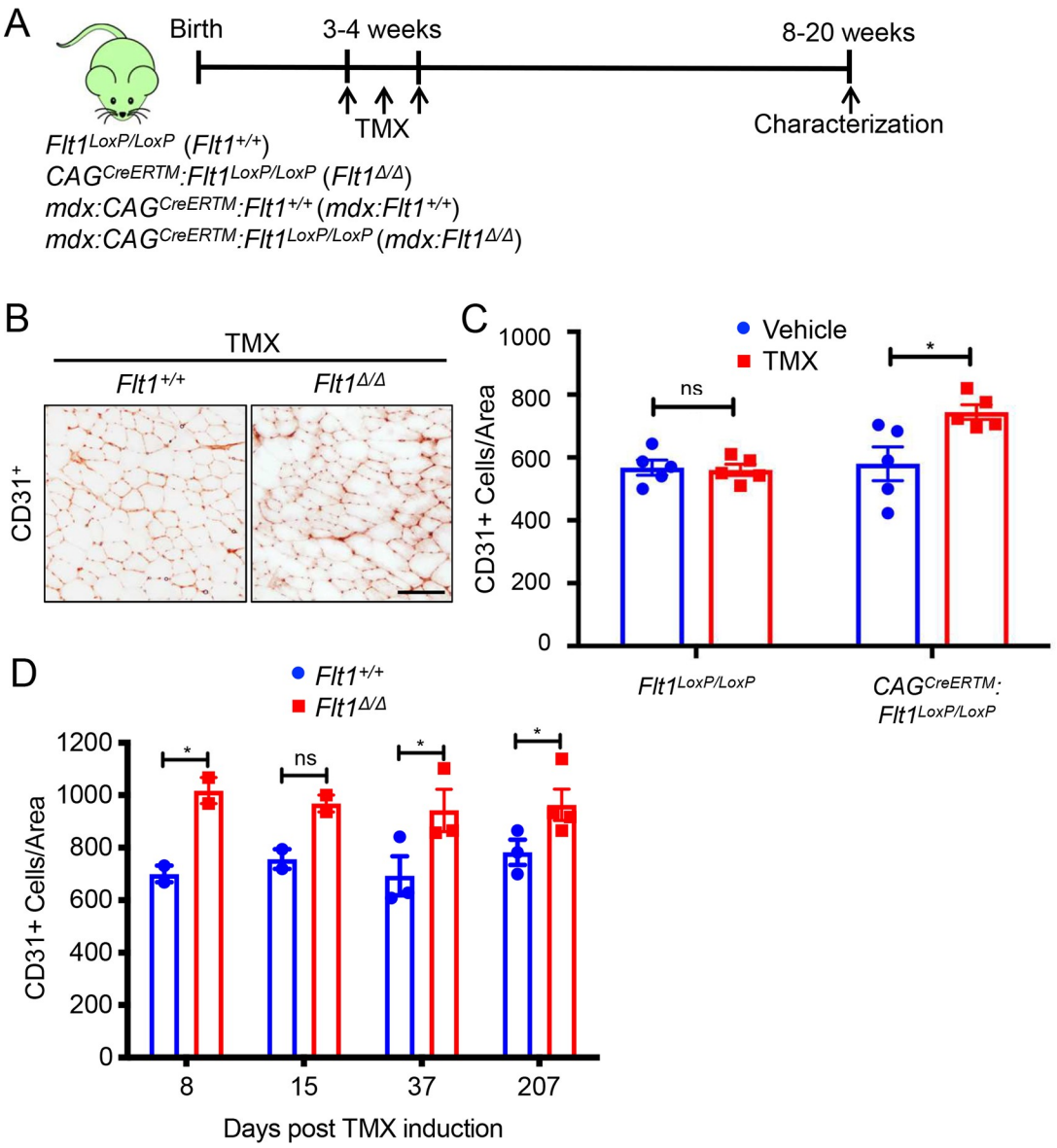

Fig 1. Postnatal deletion of *Flt1* can increase capillary density in skeletal muscle. (A) Experimental scheme for assessing angiogenic response from conditional *Flt1* deletion. (B) Representative images of CD31-stained cryosections from the TA muscle from $Flt1^{LoxP/LoxP}$ ($Flt1^{+/+}$) and $CAG^{CreERTM}$:$Flt1^{LoxP/LoxP}$ ($Flt1^{\Delta/\Delta}$) mice following tamoxifen (TMX) induction. Scale bar indicates 100 μm. (C) Increase in capillary density is dependent on $CAG^{CreERTM}$ as well as TMX induction in the $Flt1^{LoxP/LoxP}$ background. (D) Increase in capillary density is rapid and sustained following TMX induction in $Flt1^{\Delta/\Delta}$ mice more than 6 months following induction.

https://doi.org/10.1371/journal.pgen.1008468.g001

density by loss of the *Flt1* gene shown in Fig 1A was maintained in the *mdx* background in the *mdx*:$Flt1^{\Delta/\Delta}$ mice (Fig 2A and 2B). This was accompanied by a physiological increase in skeletal muscle perfusion as shown by laser Doppler imaging (Fig 2C). Next, we proceeded to look for dystrophinopathy-related muscle changes in the adult *mdx*:$Flt1^{\Delta/\Delta}$ mice. The *mdx*:$Flt1^{\Delta/\Delta}$ mice showed a shift in fiber type composition toward increases in oxidative type I slow fibers (S3B and S3C Fig). This was more pronounced in the EDL compared to the soleus, which is already predominantly type I. This large shift to type I fibers was expected as increased vascularization has been shown prior to fiber type change [22]. The type 1 fibers have been shown to be spared until

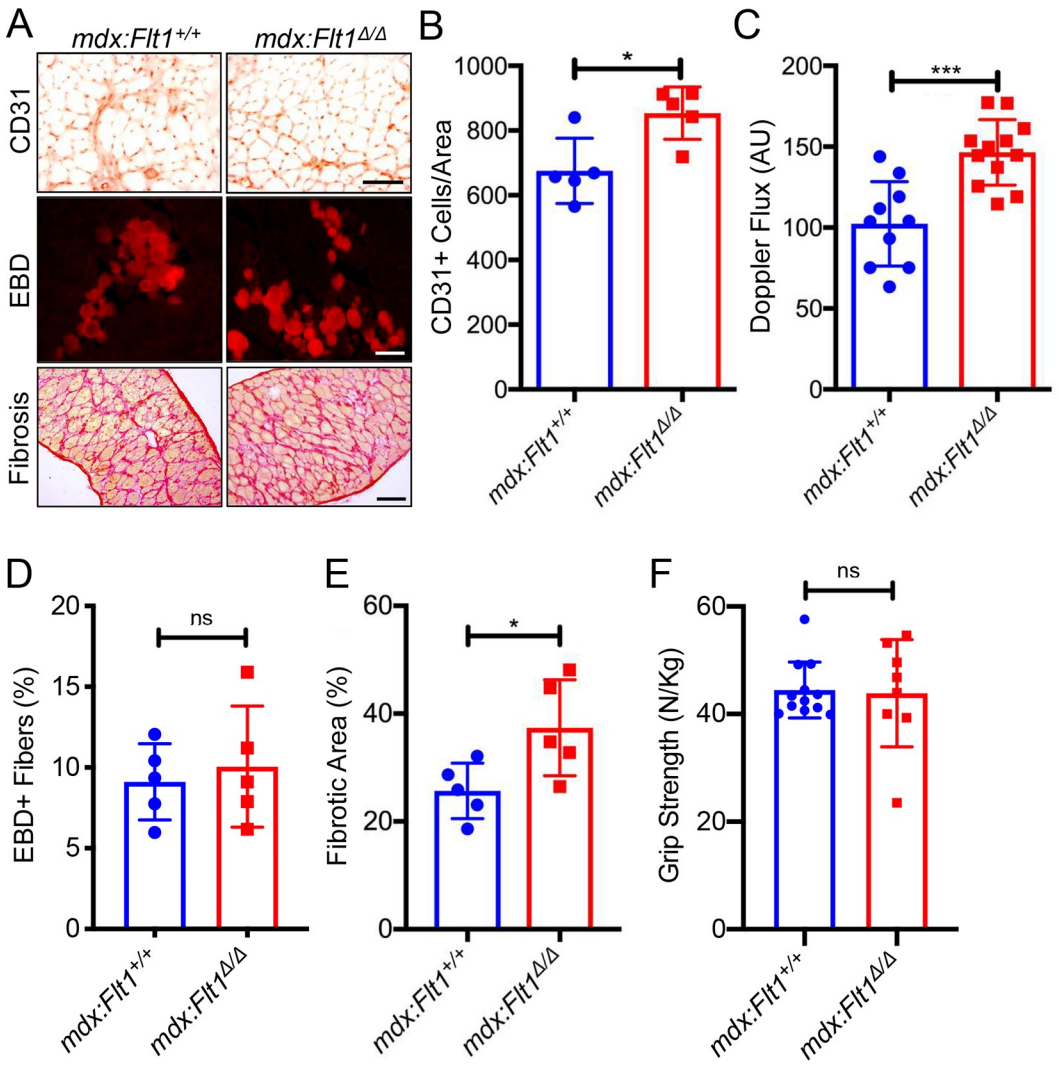

Fig 2. Increased angiogenesis is accompanied by worsened muscle pathology in the *mdx:Flt1*$^{\Delta/\Delta}$ mice. (A) Representative images of CD31-stained TA muscle, Evans blue dye (EBD) to measure acute damage in diaphragm and Sirius red staining to measure fibrosis in diaphragm. Scale bars indicate 100 μm. (B) Capillary density is increased in in the TA muscle *mdx:Flt1*$^{\Delta/\Delta}$ mice. (C) Skeletal muscle perfusion is increased in the TA muscle in *mdx:Flt1*$^{\Delta/\Delta}$ mice. (D) *mdx:Flt1*$^{\Delta/\Delta}$ mice show no difference in acute damage as judged by EBD. (E) *mdx:Flt1*$^{\Delta/\Delta}$ mice show increased in fibrosis as evaluated by Sirius red staining. (F) *mdx:Flt1*$^{\Delta/\Delta}$ mice show no difference in the grip strength normalized to body weight.

https://doi.org/10.1371/journal.pgen.1008468.g002

late in DMD and are regarded as more injury resistant [23, 24]. Evans blue dye (EBD) accumulation [25] showed no differences, while fibrosis was markedly increased in the *mdx:Flt1*$^{\Delta/\Delta}$ mice (Fig 2A, 2D and 2E). Embryonic MHC (eMHC)+ muscle fibers were increased in the *mdx:Flt1*$^{\Delta/\Delta}$ mice (S3D and S3E Fig), suggesting increased muscle fiber regeneration. There is no improvement in grip strength generation by the mice (Fig 2F). Taken together, the *mdx:Flt1*$^{\Delta/\Delta}$ mice showed that even though there was an increase in capillary density, muscle pathology worsened.

Endothelial cell-specific loss of *Flt1* in *mdx* improves muscle phenotype in *mdx* mice

Flt1 is expressed in several cell types including endothelial cells, myeloid cells and some neurons. Thus, we hypothesized that *Flt1* may be indispensable in one of these other

compartments. Since endothelial cell-specific *Flt1* deletion resulted in increased capillary density in heart and adipose tissue [20, 26], we hypothesized that deletion of endothelial cell-specific *Flt1* would be sufficient to increase angiogenesis and improve muscle pathology in the *mdx* mice.

We attempted to increase the angiogenesis in skeletal muscle using an endothelial cell-specific *VE-cadherin (Cdh5)-CreERT2*-mediated *Flt1* deletion in mice. *Cdh5* is an endothelial cell-specific cadherin gene used for lineage tracing and conditional deletion of endothelial cells [27]. Goel et al. recently reported the presence of Cdh5 in satellite cells questioning the validity of using $Cdh5^{CreERT2}$ in skeletal muscle tissue [28]. We verified the endothelial cell specificity of the $Rosa26R^{mTmG}$ reporter, and Cre-mediated excision resulted in the mGFP expression in the endothelial cells but no other cell types (S4A, S4B and S4C Fig). We saw no difference in the body mass or muscle mass in endothelial cell-specific *Flt1* deleted mice compared with the control mice (S4D and S4E Fig).

We crossed the *mdx*:$Flt1^{LoxP/LoxP}$ mice to the $Cdh5^{CreERT2}$ mice to yield the *mdx*:*Cdh5-*$Flt1^{\Delta/\Delta}$ mice (Fig 3A). Upon TMX treatment, capillary density was increased in the skeletal muscle in *mdx*:*Cdh5-*$Flt1^{\Delta/\Delta}$ mice compared with *mdx*:*Cdh5-*$Flt1^{+/+}$ mice, indicating that endothelial cell-specific deletion of *Flt1* was sufficient to increase capillary density in the skeletal muscle (Fig 3B and 3C). This was accompanied by a physiological increase in skeletal muscle perfusion using laser Doppler (Fig 3D). Moreover, the *mdx*:*Cdh5-*$Flt1^{\Delta/\Delta}$ did not show any significant changes in body and muscle mass loss (S5 Fig). Signs of DMD-associated pathology such as increased EBD uptake and fibrosis were significantly reduced in the *mdx*:*Cdh5-*$Flt1^{\Delta/\Delta}$ mice (Fig 3B, 3E and 3F). The muscle fibers in the *mdx*:*Cdh5-*$Flt1^{\Delta/\Delta}$ mice had decreased centrally located nuclei and maintained larger muscle fibers compared with the *mdx*:*Cdh5-*$Flt1^{+/+}$ mice (Fig 4A–4C). The *mdx*:*Cdh5-*$Flt1^{\Delta/\Delta}$ mice showed increased grip strength compared with the *mdx*:*Cdh5-*$Flt1^{+/+}$ mice (Fig 4D). To examine whether the number of satellite cells were affected in the *mdx*:*Cdh5-*$Flt1^{\Delta/\Delta}$ mice, the Pax7+ satellite cells located underneath basal lamina (laminin+) was quantified in TA muscle sections (Fig 4E and 4F). Interestingly, Pax7+ satellite cell population was increased in the *mdx*:*Cdh5-*$Flt1^{\Delta/\Delta}$ mice compared with the control *mdx*:*Cdh5-*$Flt1^{+/+}$ mice, indicating that an increased vascular niche might promote myogenic precursor cell proliferation and/or survival, leading to improved muscle pathology in the *mdx* mice. Taken together, these data indicate that endothelial cell-specific *Flt1* loss was sufficient to increase capillary density and result in the histological improvements correlated with a functional improvement in the *mdx* mice.

Pharmacological inhibition of FLT1 improved *mdx* mice

The genetic model of *Flt1* deletion showed an ameliorated phenotype in the *mdx* mice. To translate our genetic results into therapeutic approaches for DMD model mice, we utilized a previously reported anti-FLT1 hexapeptide (Gly-Asn-Gln-Trp-Phe-Ile or GNQWFI) that inhibits VEGF-binding to FLT1. Intramuscular administration of the anti-FLT1 peptide in TA muscle of perinatal *mdx* mice (S6A Fig) increased capillary density and decreased muscle pathology in the treated muscle (S6B–S6D Fig). We assessed the diaphragm muscle after systemic (intraperitoneal; IP) injection of the anti-FLT1 peptide at a low (10 mg/kg body weight) and a high dose (100 mg/kg body weight) to test for therapeutic potential in *mdx* mice (Fig 5A). There was no significant body mass alteration following anti-FLT1 peptide treatment (S6E and S6F Fig). While treatment with a low dose of anti-FLT1 peptide had no effect on capillary density, skeletal muscle perfusion, membrane permeability or fibrosis, the high dose increased capillary density and skeletal muscle perfusion, and decreased EBD+ fibers and fibrosis (Fig 5B–5F). Importantly, the high dose of anti-FLT1 peptide also increased muscle

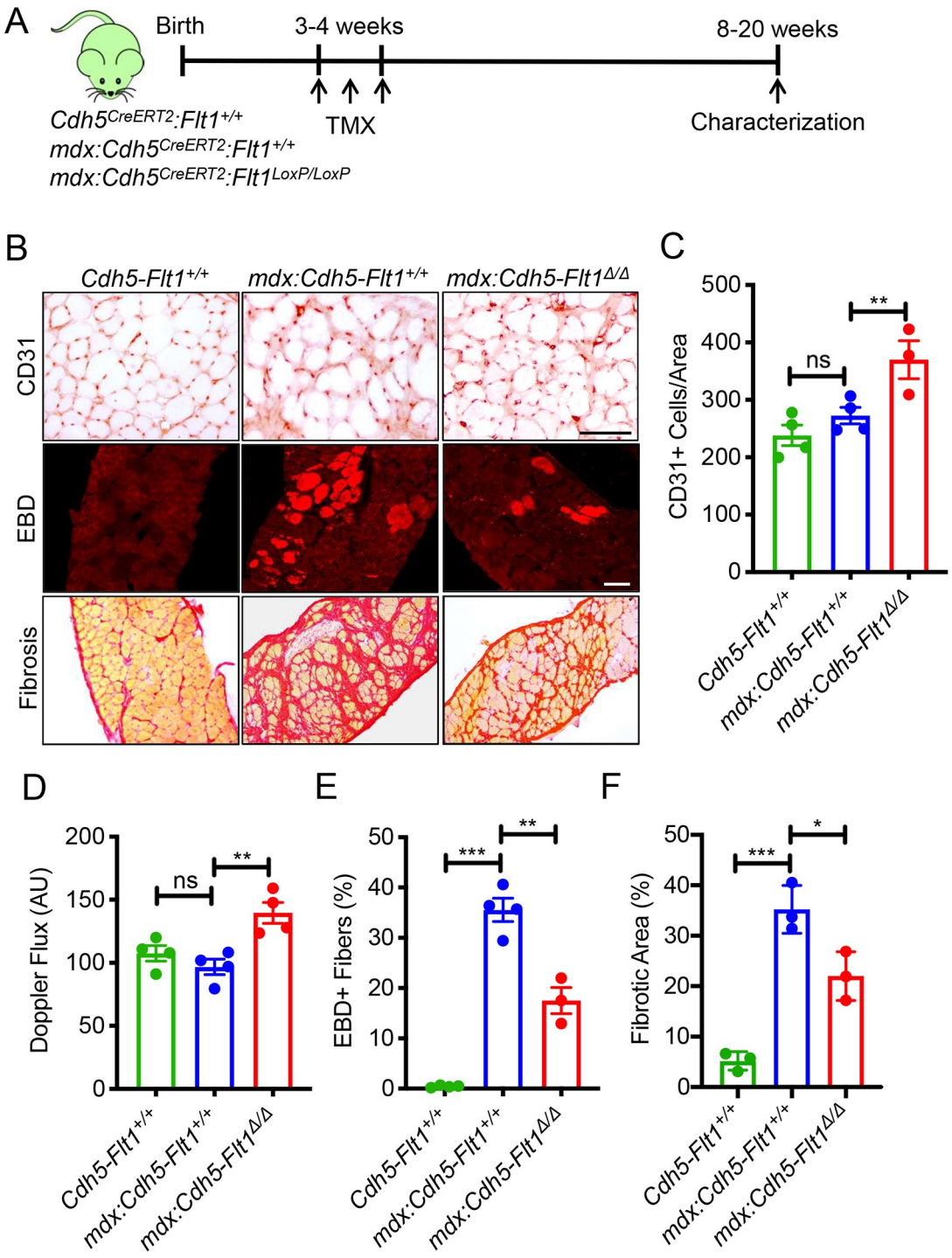

Fig 3. Endothelial cell-specific conditional deletion of *Flt1* in *mdx*:*Cdh5-Flt1*$^{\Delta/\Delta}$ mice improve capillary density and muscle phenotype. (A) Experimental scheme for assessing angiogenic response from conditional *Flt1* deletion. *Cdh5-Flt1*$^{+/+}$ and *mdx*:*Cdh5-Flt1*$^{+/+}$ mice were used as wild-type and *mdx* controls, respectively. (B) Representative images of CD31 staining for capillary density, Sirius red staining to measure fibrosis and EBD to measure acute damage in the diaphragm. Scale bars indicate 100 μm. (C) Endothelial cell specific conditional deletion of *Flt1* (*mdx*:*Cdh5-Flt1*$^{\Delta/\Delta}$) is sufficient to increase the capillary density in diaphragm. (D) Endothelial cell specific conditional deletion of *Flt1* (*mdx*:*Cdh5-Flt1*$^{\Delta/\Delta}$) is sufficient to increase skeletal muscle perfusion. (E) Acute damage as judged by EBD is reduced in *mdx*:*Cdh5-Flt1*$^{\Delta/\Delta}$ mouse muscle. (F) Fibrosis is reduced in *mdx*:*Cdh5-Flt1*$^{\Delta/\Delta}$ mouse muscle as evaluated by Sirius red staining.

https://doi.org/10.1371/journal.pgen.1008468.g003

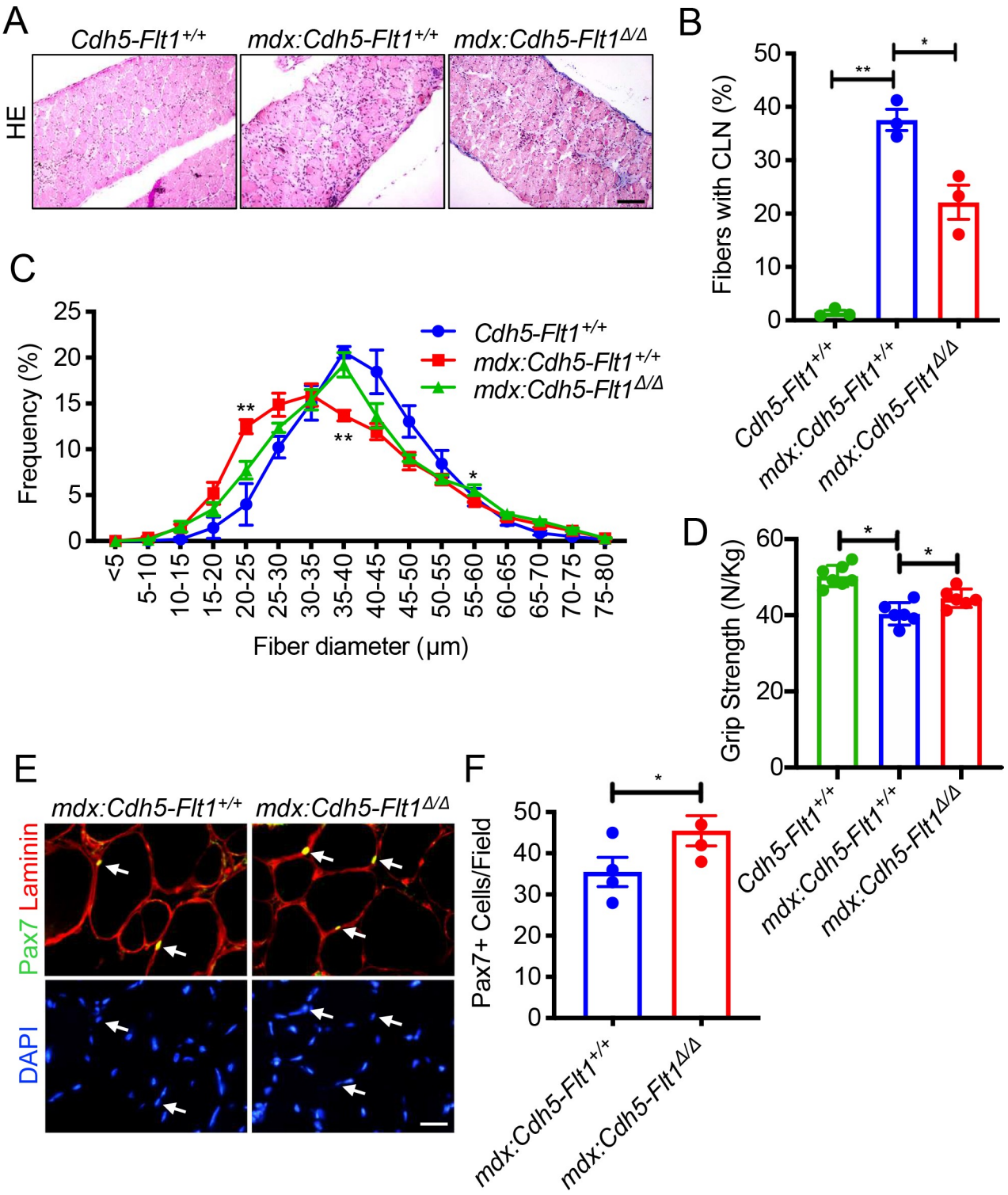

Fig 4. Endothelial cell-specific conditional deletion of *Flt1* in *mdx*:*Cdh5-Flt1*$^{\Delta/\Delta}$ mice improve muscle histology and function. (A) Representative images of HE staining of diaphragm. Scale bar indicates 100 μm. (B) Diaphragm muscle fiber turnover is reduced in *mdx*:*Cdh5-Flt1*$^{\Delta/\Delta}$ mouse muscle as evaluated by centrally located nuclei (CLN). (C) Distributions of mean fiber diameter in TA muscle of *mdx*:*Cdh5-Flt1*$^{\Delta/\Delta}$ mice were skewed toward the bigger fiber size compared with the control *mdx*:*Cdh5-Flt*$^{+/+}$ mice. Stastical comparisons were examined in between *mdx*:*Cdh5-Flt1*$^{+/+}$ and *mdx*:*Cdh5-Flt1*$^{\Delta/\Delta}$ mice. (D) Grip strength is increased in *mdx*:*Cdh5-Flt1*$^{\Delta/\Delta}$ mice normalized to body weight. (E) Representative images from TA muscle of *mdx*:*Cdh5-Flt1*$^{\Delta/\Delta}$ mice stained with anti-Pax7 antibody (yellow) to detect satellite cells (arrows) and anti-laminin antibody (red) to detect basal lamina. Nuclei were counterstained with DAPI (blue). Scale bar indicates 20 μm. (F) Quantification of Pax7+ myogenic cells in a TA muscle. Relative amount of Pax7+ cells counted in a view field.

https://doi.org/10.1371/journal.pgen.1008468.g004

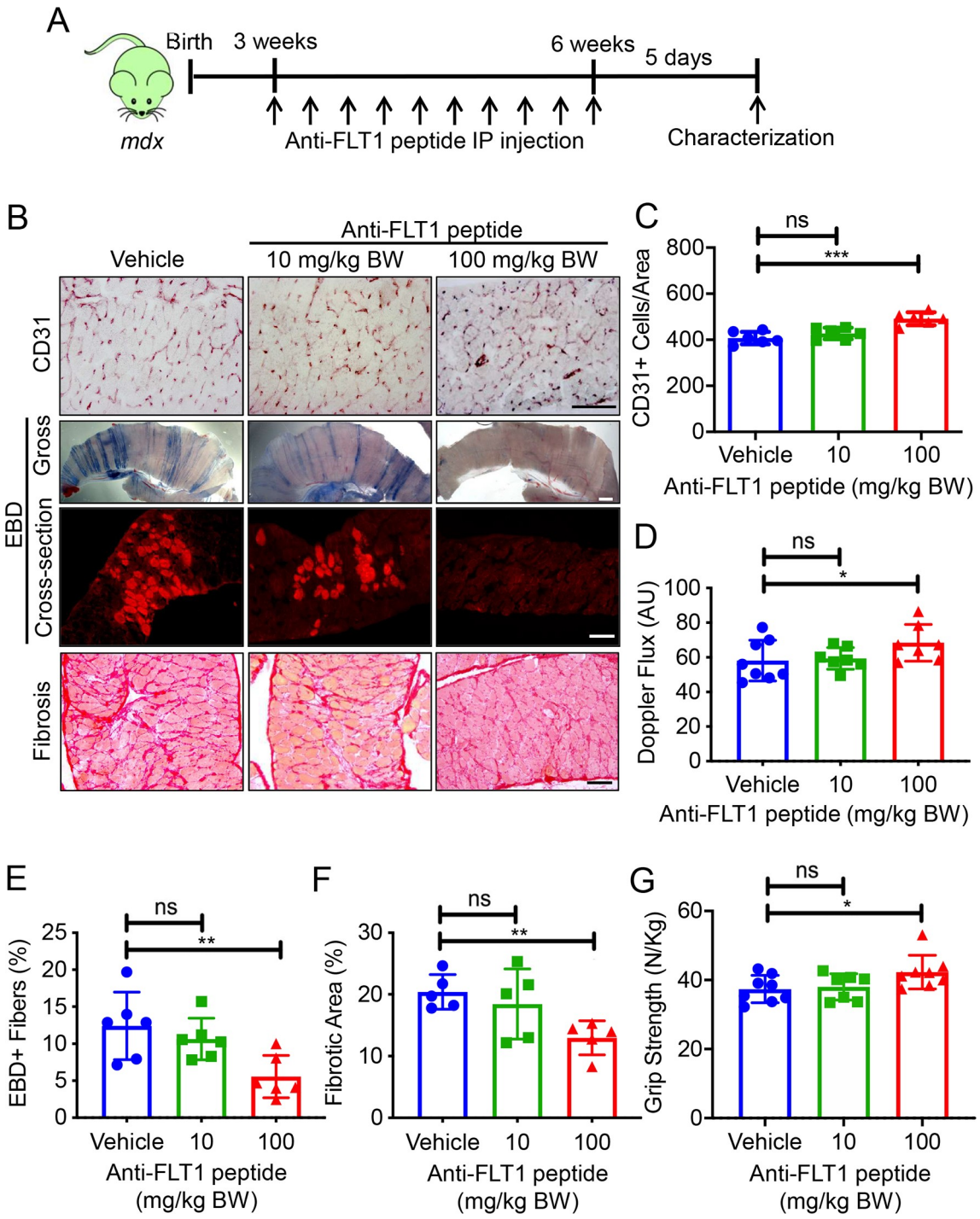

Fig 5. Systemic anti-FLT1 peptide improves skeletal muscle pathology in *mdx* mice. (A) Experimental scheme for treatment of *mdx* mice with systemic treatment using anti-FLT1 peptide. (B) Representative images of (top) CD31, (middle) gross whole mount and cryosections for EBD, (bottom) Sirius red staining of diaphragm in *mdx* mice treated with anti-FLT1 peptide. Scale bars indicate 100 μm. (C) Anti-FLT1 peptide injection increases capillary density in the *mdx* mouse muscle at high dose. (D) Anti-FLT1 peptide injection is sufficient to increase skeletal muscle perfusion in *mdx* mice at high dose. (E) Anti-FLT1 peptide injection decreases EBD + area in the *mdx* mouse muscle at high dose. (F) Anti-FLT1 peptide injection decreases fibrotic area in the *mdx* mouse muscle at high dose. (G) Grip strength is improved by anti-FLT1 peptide injection at high dose in *mdx* mice normalized to body weight.

https://doi.org/10.1371/journal.pgen.1008468.g005

stability since regenerating muscle fibers which have centrally located nuclei and eMHC+ fibers were decreased (S7A–S7C Fig). Consequently, anti-FLT1 peptide-treated *mdx* mice increased grip strength compared with the control *mdx* mice (Fig 5G). Since FLT1 is also detected in myeloid cells and motor neurons, systemic anti-FLT1 peptide might induce blood phenotypes and motor behavioral abnormality. However, we did not see changes in myeloid cell numbers in their peripheral blood or changes in motor coordination on the Rotarod test in *mdx* mice (S7A and S7D Fig).

To increase stability and the hydrophobicity [29], we tested a D-isoform anti-FLT1 peptide attached to polyethylene glycol (PEG). However, systemic administration of the PEG-D-form anti-FLT1 peptide did not increase capillary density or improve muscle pathology or function in the *mdx* mice (S8 Fig). Taken together, these proof-of-concept experiments showed that postnatal inhibition of FLT1 by anti-FLT1 peptide could ameliorate the pathology associated with DMD in the *mdx* mice. However, the functional dose (100 mg/kg body weight) was orders of magnitude higher than the generally acceptable pharmacological standards of body weight dosage for small molecule drugs [30]. Therefore, a more potent or alternative strategy is required for further translational studies.

Screening for an antibody against FLT1

As postnatal gene deletion and pharmacological inhibition of FLT1 decreased the muscular dystrophy-associated pathology in the *mdx* mice, we next sought to examine whether it could do this in a more translational manner using biologics to block FLT1. To establish proof of principle, we screened 8 commercially available MAbs that could block VEGF-FLT1 binding. We first screened for the ability of the MAbs to block chimeric FLT1-FC binding to PlGF2, a VEGF family protein, using ELISA (S9A and S9B Fig), since both PlGF2 and VEGFA occupy the same binding sites on the extracellular domain of FLT1 [31]. Three MAbs showed higher binding affinities: EWC (Novus Biologicals), MAB0702 Mab (Angio-Proteomie) and EWC (Acris GmbH) blocked binding by 65.4%, 64.8%, and 60.6%, respectively, while the control polyclonal anti-FLT1 antibody could block 83.1% of binding (S9B Fig). We selected two MAbs (MAB0702 from Angio-Proteomie and EWC from Novus Biologicals) for further analyses based on their blocking efficiency and their availability for large *in vivo* studies. The MAB0702 and EWC were raised against the extracellular domains of the human FLT1, and likely target both membrane-bound (mFLT1) and sFLT1 due to similar homology of epitopes. We validated the blocking affinity to VEGFA-FLT1 binding, and found that MAB0702 and EWC blocked binding by 40.1% and 19.9%, respectively, compared to the 94.3% for the polyclonal control (S9B Fig). We further determined the antibodies' affinities against mouse and human FLT1-FC protein using Biacore analysis (S2 Table). MAB0702 and EWC had similar association rate/binding constants (Ka) for both mouse and human FLT1-FC. By contrast, MAB0702 had significantly higher dissociation constants (Kd) and equilibrium dissociation constants (KD) for mouse FLT1-FC compared with EWC, while MAB0702 had lower dissociation constants (Kd) and equilibrium dissociation constants (KD) for human FLT1-FC compared with EWC. Based on these affinity studies, we decided to utilize both MAB0702 and EWC MAbs for *in vivo* experiments.

Testing Anti-FLT1 antibody treatment for *mdx* mice

We intravenously (IV) injected MAB0702 at a dose of 20 mg/kg body weight into *mdx* mice, and measured free sFLT1 and VEGFA in the serum. We found a significant decrease in free serum sFLT1 (S9C Fig) and an increase in serum VEGFA levels (S9D Fig) following MAB0702 injection, suggesting the efficient blocking of MAB0702 to sFLT1 and FLT1 *in vivo*. Based on

our screening results, *mdx* mice were injected with IV MAbs or isotype control IgG dosing at 20 mg/kg body weight every 3 days for four weeks beginning at 3 weeks of age (Fig 6A). The treatment with MAB0702 at 20 mg/kg body weight but not EWC or isotype control significantly increased capillary density and skeletal muscle perfusion using laser Doppler (Fig 6B–6D). More importantly, the mice treated with MAB0702 at 20 mg/kg body weight also displayed improved histology, such as decreased number of EBD+ fibers, decreased fibrosis, decreased calcification, and decreases in CLN (Figs 6B, 6E–6G, 7A and 7B) without affecting any body weight compared with the *mdx* mice (S9E and S9F Fig). Treatment prevented the increase in smaller caliber muscle fibers seen in the *mdx* mice (Fig 7A and 7C). While the EWC had significantly lower dissociation constants to mouse FLT1 compared with MAB0702 (S2 Table), we were surprised to find that *in vivo* administration of the EWC did not induce changes in capillary density, skeletal muscle perfusion or muscle pathology (Figs 6B, 6C–6G, 7A, 7B). MAB0702-treated *mdx* mice generated increased grip strength compared with the *mdx* mice (Fig 7D). Skeletal muscle endurance, as assessed by treadmill running as an indicator of maximal muscle capacity, showed running duration and distance of MAB0702-treated *mdx* mice significantly increased compared to *mdx* mice (Fig 7E and 7F). Thus, anti-FLT1 antibody administration depleted sFLT1 levels and increased free serum VEGFA levels, which led to increased angiogenesis and reduced muscle pathology in *mdx* mice, providing a potential new pharmacological strategy for treatment of DMD. To examine whether the number of satellite cells was affected in the MAB0702-treated *mdx* mice, the Pax7+ cells located underneath basal lamina was quantified in TA muscle sections (Fig 7G and 7H). Importantly, Pax7 + satellite cells were increased in the MAB0702-treated *mdx* mice compared with the control *mdx* mice. Taken together, these data strongly indicate that pharmacological inhibition of FLT1 may benefit patients with DMD by either increasing VEGFA and/or decreasing sFLT1 as a therapeutic target.

Discussion

We have previously shown that *mdx* mice carrying heterozygous global deletion of *Flt1* display increased capillary density, and improved muscle pathology [14]. In this report we show the effect of modulating Flt1 using several different techniques and mouse models (S1 Table). First, we show that *Flt1* is important postnatally as conditional *Flt1* deletion in *mdx*:*Flt1*$^{\Delta/\Delta}$ mice in the perinatal stage results in lethality in mice. While deletion of *Flt1* in neonates increased capillary density in both C57BL6 and *mdx* mice, it led to the worsening of the skeletal muscle phenotype. Since *Flt1* is expressed in several cell types including endothelial cells, myeloid cells and some neurons [16–18, 27], *Flt1* may be indispensable in one of these other compartments when both alleles are perinatally deleted. For example, *Flt1* is expressed in motor neurons, where is not simply acting as a VEGFA sink-trap. In motor neurons, tyrosine kinase activity of Flt1 is required for their survival [17]. Thus, the observed increased angiogenesis but worse pathological alterations in *mdx*:*Flt1*$^{\Delta/\Delta}$ muscle may be due to motor neuron–associated changes. By contrast, loss of *Flt1* in endothelial cells in the postnatal stage increased the capillary density and blood perfusion in skeletal muscle without significant decreases in weight or muscle mass. Increased angiogenesis and blood perfusion were observed in the global *Flt1* heterozygous knockout mice [15], indicating that loss of endothelial cell-specific *Flt1* in *mdx*:*Cdh5-Flt1*$^{\Delta/\Delta}$ mice was sufficient to produce increased capillary density and vascular perfusion in the skeletal muscle. This also led to an improved *mdx*-associate muscle pathology, confirming that postnatal deletion of *Flt1* is able to rescue the dystrophinopathy related muscle pathology.

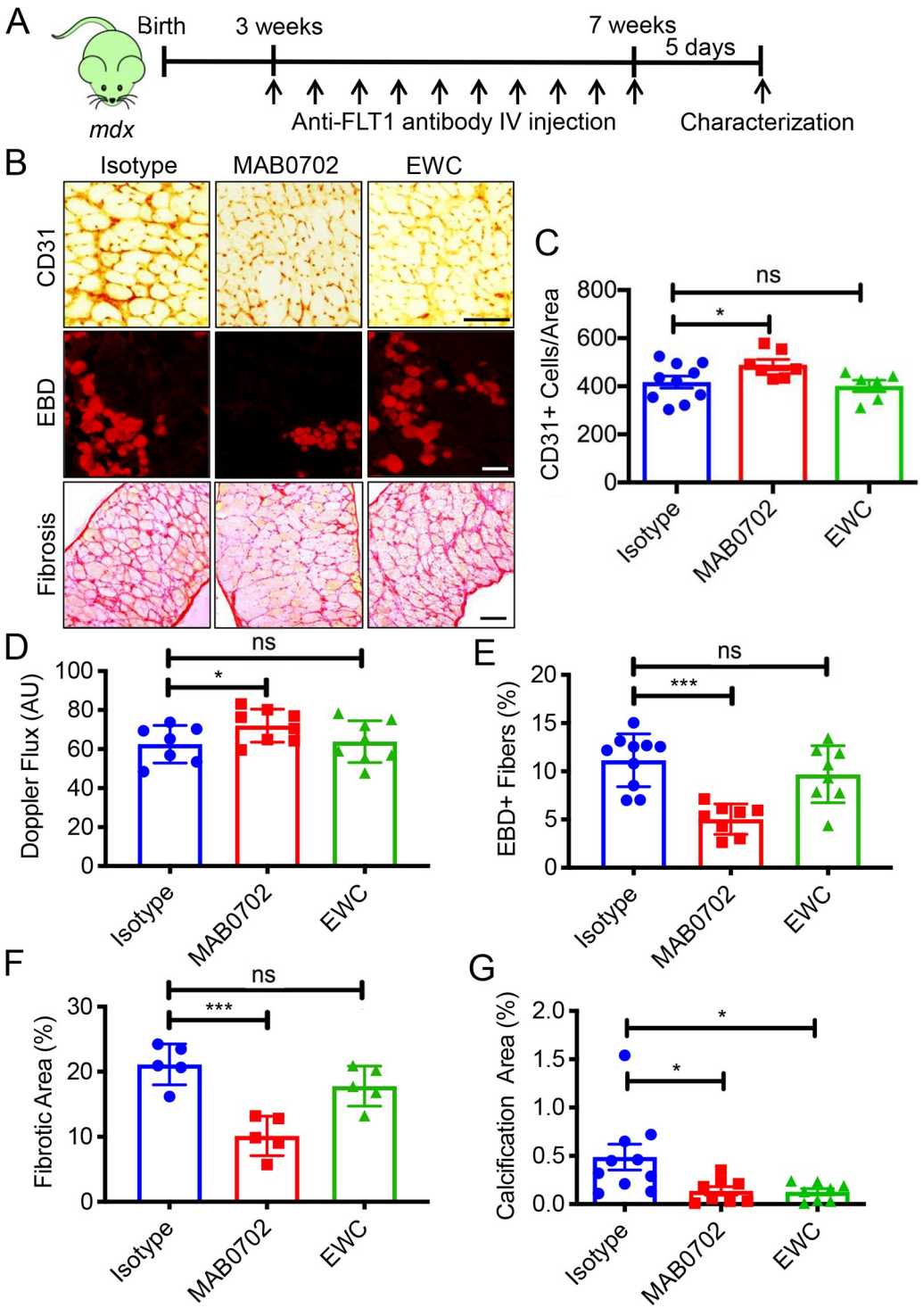

Fig 6. MAbs against FLT1 for the treatment of muscular dystrophy in the *mdx* mice. (A) Experimental scheme for systemic treatment of *mdx* mice with systemic injection of anti-FLT1 antibody. (B) Representative images of (top) CD31, (middle) EBD and (bottom) Sirius red staining of diaphragm in *mdx* mice treated with anti-FLT1 antibody. Scale bars indicate 100 μm. (C) Capillary destiny is increased in MAB0702 treated mice but not EWC in *mdx* mice compared with isotype control. (D) MAB0702 but not EWC injection is sufficient to increase skeletal muscle perfusion in *mdx* mice. (E) EBD+ area is decreased in MAB0702 treated mice but not EWC in *mdx* mice compared with isotype control. (F) Fibrotic area is decreased in MAB0702 treated mice but not EWC in *mdx* mice compared with isotype control. (G) Calcification is decreased in both MAB0702 and EWC treated mice in *mdx* mice compared with isotype control.

https://doi.org/10.1371/journal.pgen.1008468.g006

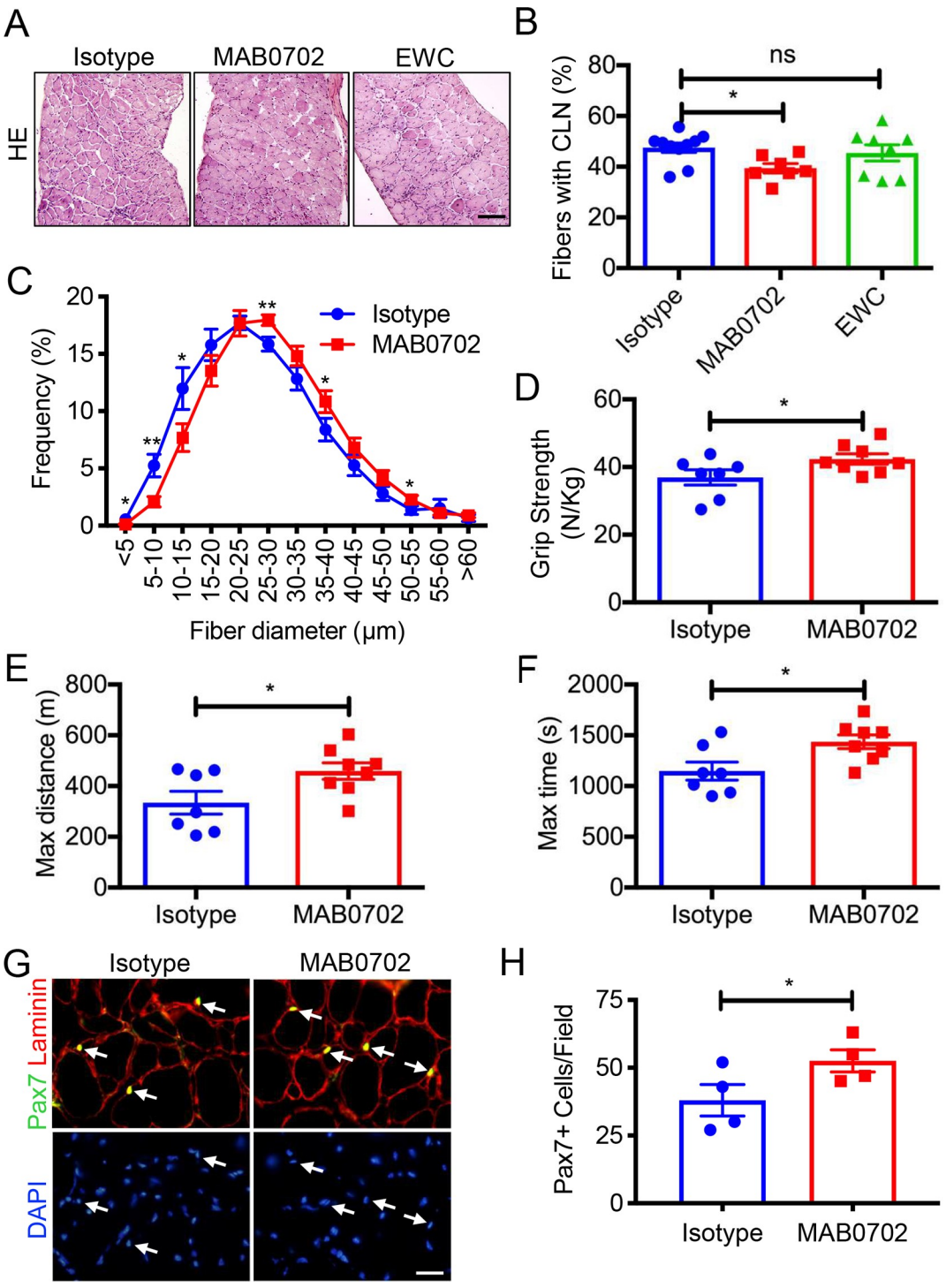

Fig 7. Systemic delivery of MAbs against FLT1 improves skeletal muscle pathology in *mdx* mice. (A) Representative images of HE staining of diaphragm in *mdx* mice treated with anti-FLT1 antibodies. Scale bars indicate 100 μm. (B) Diaphragm muscle fiber turnover is reduced in MAB0702 treated *mdx* mouse muscle as evaluated by centrally located nuclei (CLN). (C) Distributions of mean fiber diameter in TA muscle of MAB0702 treated *mdx* mice were skewed toward the bigger fiber size compared with compared with isotype control. (D) Grip strength is improved in *mdx* mice treated with MAB0702 compared with isotype control. (E, F)Treadmill running time and distance are improved in *mdx* mice following MAB0702 treatment. (G) Representative images from TA muscle of MAB0702 treated *mdx* mice stained with anti-Pax7 antibody (yellow) to detect satellite cells (arrows) and anti-laminin antibody (red) to detect basal lamina. Nuclei were counterstained with DAPI (blue). Scale bar indicates 20 μm. (H) Quantification of Pax7+ myogenic cells in a TA muscle. Relative amount of Pax7+ cells counted in a view field.

https://doi.org/10.1371/journal.pgen.1008468.g007

Importantly, for the first time, we demonstrated that administration of both anti-FLT1 peptide and anti-FLT1 MAb increased angiogenesis, which led to an improved the pathology associated with DMD in *mdx* mice, and is a phenocopy of our genetic models (*mdx*:*Cdh5-Flt1*$^{\Delta/\Delta}$ mice). Notably, the improved DMD pathologies via systemic pharmacological inhibition of Flt1 were the phenocopy seen in *mdx*:*Cdh5-Flt1*$^{\Delta/\Delta}$ mice but not observed in *mdx*:*Flt1*$^{\Delta/\Delta}$ mice which showed markedly worsened muscle pathology. This contradiction may be partly due to the fact that anti-FLT1 peptide and MAb may be unable to target the membrane associated FLT1 in the motor neurons, which might prevent the mice from motor neuron–associated changes [32–34]. We screened commercially available MAbs for blocking ligands-FLT1, and demonstrated that administration of MAB0702 MAbs was able to phenocopy our genetic model in a manner suited for translational studies to reduce muscle pathology in *mdx* mice.

After MAB0702 administration, we showed a small increase in VEGFA levels in serum. It should be noted that a mere 2-fold increase of VEGFA during development is incompatible with life in transgenic mice [35]. Computation and experimental models showed that local VEGF gradients are more important than the total concentration [36, 37]. We recently demonstrated that muscle satellite cells express abundant VEGFA, which recruits endothelial cells and capillaries to the proximity of satellite cells on muscle fibers [38]. Taken together, these data strongly suggest that hot-spots with high levels of VEGFA in *Flt1* knockout or anti-FLT1 treated mice may result in increased capillary density and vascular perfusion, which is predicted to result in decreased associated DMD-type pathological changes in the skeletal muscles. Improvement of dystrophic muscle function by FLT1 blockade may provide a novel pharmacological strategy for treatment of diseases associated with DMD via increased serum and tissue VEGFA levels, which induce increased vascular density and perfusion.

While VEGFA binds to both FLT1 and FLK1, VEGFB, PlGF1 and PlGF2 only bind to FLT1 [39]. This creates a scenario where PlGF1/2 and VEGFB binding can sequester FLT1, increasing serum and tissue VEGFA availability for VEGFA-FLK1 binding-mediated angiogenic induction. While *PlGF* is dispensable for normal development and health, and not expressed in the normal adult tissues outside the female reproductive organs [40], VEGFB is expressed in the muscle tissue and muscle fibers [41]. VEGFB may play a role in diet induced obesity and free fatty acid uptake by the endothelial cells in skeletal muscle [42], but this remains controversial [26]. However, VEGFB overexpression does not result in an angiogenic response in ischemic skeletal muscle [43], indicating that blocking VEGFB-FLT1 signaling is not likely to be responsible for the angiogenic changes seen in this study.

The present study shows that increased angiogenesis may be a novel avenue to improve some of pathology associated with loss of dystrophin, including function, and could be used in conjunction with other treatment strategies. For example, intramuscular injection of VEGF containing recombinant adeno-associated viral vectors resulted in both functional and histological improvements in both ischemic and *mdx* muscle [44–47]. This improvement was seen in combination with increased in angiogenesis in the muscle. Increased capillary density in the *mdx* muscle work through paracrine stimulation, by protecting muscle fiber damage and promoting satellite cell proliferation, survival and self-renewal in the vascular niche [38, 48]. Indeed, we demonstrated that Pax7+ satellite cell population was increased in the *mdx*:*Cdh5-Flt1*$^{\Delta/\Delta}$ mice and the MAB0702-treated *mdx* mice. Christov et al. and our group showed that satellite cells were preferentially located next to capillaries [38, 49]. Since our approaches increased the number of capillaries found in the examined muscles, it may effectively increase the amount of vascular niche that houses the satellite cell compartment in the muscle. Recently, we showed that genes encoding for endothelial and satellite cells were highly correlated across muscle groups, and endothelial cells could mediate satellite cell self-renewal via Notch activation [38]. Therefore, increase in the vascular niche may increase satellite cell self-

renewal and the number of myogenic precursor cells, which we hypothesize may be responsible for the improved phenotype seen in the *mdx* mice with *Flt1* deletion or functional blockage.

MAb-based therapeutics for the treatment of DMD have been developed to increase muscle mass via targeting myostatin and to decrease fibrosis via targeting fibroadipogenic progenitors [50]. Further optimization using with humanized antibodies are required for future translation to humans [51]. Taken together, we have gathered evidence for the first time that FLT1-targeted MAbs may be an effective therapeutic approach for the treatment of DMD.

Methods

Mice

Flt1$^{Loxp/Loxp}$ mice were obtained from Dr. Gua-Hua Fong [20]. *Cdh5*^{CreERT2} mice were obtained from Dr. Yoshiaki Kubota [27]. B6Ros.Cg-*Dmd*$^{mdx\text{-}5Cv}$/J (*mdx*; JAX stock #002379) [52], B6.Cg-Tg(CAG-cre/Esr1*)5Amc/J (*CAG*^{CreERTM}; JAX stock #004682) [19] and D2.129 (Cg)-*Gt(ROSA)26Sor*$^{tm4(ACTB\text{-}tdTomato\text{-}EGFP)Luo}$/J (*Rosa26R*^{mTmG}; JAX stock #007576) [53] mice were obtained from Jackson Laboratory. All the mice used in this study were listed in S1 Table. Colonies for all the mice were established in the laboratory. Cre recombination was induced using tamoxifen (TMX) (T5648, MilliporeSigma) dosed as 75 mg/kg body weight x 3 time over one week at 3–4 weeks of age unless otherwise specified. We also injected 4-hydroxy tamoxifen (4-OHT) (H6278, MilliporeSigma) dosed as 25 mg/kg body weight. Control mice contained the wild-type (WT) *CreER* allele or were injected with the vehicle (corn oil or 10% ethanol).

Ethical Statement

All animal studies were approved by the IACUC at University of Minnesota (190336906A).

Anti-FLT1 peptides and antibodies

The anti-FLT1 peptide was synthesized from Peptide 2.0 Inc. based on the sequence (Gly-Asn-Gln-Trp-Phe-Ile or GNQWFI) as previously described [54]. DMSO was used to dissolve the peptide. Twenty μg of peptide diluted in 2% DMSO in PBS solution was used for intramuscular injection per day in the TA muscle. Ten mg/kg body weight and 100 mg/kg body weight were used for the systemic treatment via IP injection. The second generation anti-FLT1 peptide (PEG-$G_DN_DQ_DW_DF_DI_D$) was synthesized with the following modifications: The polyethylene glycol moiety was attached to the peptide to improve solubility in polar solvents and the D isomeric form was used instead of the L to enhance stability of the peptide [29]. PBS was used as a vehicle. The peptides were commercially synthesized (LifeTein, LLC). Commercially available anti-FLT1 antibodies were obtained from the manufacturer in carrier free and preservative free form (AF471 from R&D Systems, D2 from Santa Cruz Biotechnology, EWC from Acris GmbH and Novus Biologicals, LS-C6855 from LifeSpan BioSciences, MAB1664 from MilliporeSigma and MAB7072 from Angio-Proteomie, Abcam and Santa Cruz Biotechnology). Isotype IgG (Santa Cruz Biotechnology) was used for control experiment. Two or 20 mg/kg body weight was used for the systemic treatment. Retro-orbital IV injections were performed for systemic treatment for the antibody.

RNA and genomic DNA isolation and qPCR

Mouse TA muscle was homogenized in TRIzol reagent (15596026, ThermoFisher Scientific) for RNA isolation. RNA was isolated using the Direct-zol RNA Microprep Kit (R2062, Zymo Research) with on-column DNase digestion, and 1 μg RNA was used for cDNA synthesis

using the Transcriptor First Strand cDNA synthesis kit (04379012001, Roche Molecular Diagnostics) with random primers. Genomic DNA was isolated from mouse tail snips with lysis buffer containing Proteinase K (P2308, MilliporeSigma). Genotyping was performed by agarose gel electrophoresis-mediated detection following PCR reaction by Taq polymerase (M0273, New England Biolabs). qPCR was performed using GoTaq qPCR Master Mix (A6001, Promega). Primer sequences are listed in S3 Table. All primers were synthesized as custom DNA oligos from Integrated DNA technologies (IDT).

Muscle perfusion

RBC flux was evaluated using the moorLabTM laser Doppler flow meter as previously described [15]. with the MP7a probe that allows for collecting light from a deeper tissue level than standard probes according to the manufacturer's instructions (Moor Instruments). The fur from the right hind leg was removed using a chemical depilatory. Readings were taken using the probe from at least 10 different spots on the TA muscle. The AU was determined as the average AU value during a plateau phase of each measurement.

Grip strength test

Forelimb grip strength test was performed following a previously published procedure [55]. Briefly, *mdx* mice were gently pulled by the tail after fore limb-grasping a metal bar attached to a force transducer (Columbus Instruments). Grip strength tests were performed by the same blinded examiner. Five consecutive grip strength tests were recorded, and then mice were returned to the cage for a resting period of 20 minutes. Then, three series of pulls were performed each followed by 20 min resting period. The average of the three highest values out of the 15 values collected was normalized to the body weight for comparison.

Treadmill running

Exer-3/6 Treadmill (Columbus Instruments) was used for treadmill running test as previously described [56]. Briefly, for acclimation, mice were placed in each lane and forced to run on a treadmill for 5 minutes at a speed of 10 m/min on a 0% uphill grade for 3 days. And then, mice were forced to run on a treadmill with a 10% uphill grade starting at a speed of 10 m/min for 5 minutes. Every subsequent 2 minutes, the speed was increased by 2 m/min until the mice underwent exhaustion which was defined as the inability of the mice to remain on the treadmill. The time of running as well as the distance run were recorded.

Rotarod test

Mice were trained on the rotarod (0890M-D54 Rotamex-5, Columbus Instruments) for 2 days before collecting data as previously described [57]. During each trial, mice were placed on the rod at 10 rpm for 60 seconds, and the rod accelerated from 10 to 30 rpm in 30 second intervals. The total maximum testing time was 240 seconds. Each trial was done twice a day (2-hour interval between sessions) for 3 consecutive days. The latency to fall was recorded, and the longest running time was used for analysis.

Histology and immunofluorescence

To assess the microvasculature ECs, we utilized intravital tomato-lectin (DL-1178, Vector labs) staining following retro-orbital IV injections. Tissues were frozen fresh using LiN_2 chilled isopentane and stored at -80°C. Eight μm thick transverse cryosections were used for all histological analysis. Slides were fixed using 2% PFA and washed twice using PBS + 0.01% Triton

(PBST) before being used. For capillary density measurement, immunohistochemistry for CD31 was performed using anti-CD31 antibody followed by the Vectastain Elite ABC Kit (PK-6100, Vector Laboratories) according to the manufacturer's instructions and developed using 3-amino-9-ethylcarbazole (AEC) (A5754, MilliporeSigma). For immunofluorescence, sections were fixed, washed twice in PBST, incubated with 0.2% Triton X-100 for 10 min and blocked by 10% BSA. Sections were incubated with primary antibodies overnight, washed twice in PBST and incubated in fluorescent-conjugated secondary antibody for 1 hour. Anti-FLT1 (RB-9049, NeoMarkers) and anti-Laminin (4H8-2, MilliporeSigma) antibodies followed by anti-rabbit Alexa-488 and anti-rat Alexa-568 (Molecular Probes) were used for detection of FLT1 expression in capillaries. Anti-type I slow MHC (NOQ7.5.4D, MilliporeSigma) or anti-embryonic MHC (F1.652, Developmental Study Hybridoma Bank) and anti-Laminin (4H8-2, MilliporeSigma) antibodies followed by anti-mouse Alexa-488 (A21202, ThermoFisher Scientific) and anti-rat Alexa-594 antibodies (A21471, ThermoFisher Scientific) were used for detection of slow or regenerating muscle fibers. Anti-Pax7 (MAB1675, R&D Systems) and anti-Laminin (4H8-2, MilliporeSigma) antibodies followed by anti-mouse Alexa-488 (A21202, ThermoFisher Scientific) and anti-rat Alexa-594 antibodies (A21471, ThermoFisher Scientific) were used for detection of satellite cells. One percent Evans blue dye (EBD) (E2129, MilliporeSigma) dissolved in PBS were injected IP at 1% body weight 16–20 hours prior to dissecting the mouse [21]. Sirius red, Alizarin red, and Hematoxylin & Eosin (HE) were performed as previously described [14]. All sections were co-stained using DAPI and mounted using DAKO mounting media. Myeloid cells and lymphocytes were identified by May-Grunwald's Giemsa (660–75, Sigma-Aldrich). Microscopic images were captured by a DP-1 digital camera attached to BX51 fluorescence microscope with 10×, 20× or 40× UPlanFLN objectives (all from Olympus). Fiji was used for image processing [58].

Biacore Surface Plasmon Resonance (SPR) Binding Assay for Anti-FLT1 MAbs

The single cycle kinetics method was used for sFLT1 binding assay by Biacore (GE Healthcare Bio-Science). A CM5 series S sensor chip (GE Healthcare Bio-Science) with mouse and human soluble FLT1-FC chimeric protein (471-F1-100 and 321-FL-050/CF, R&D Systems) immobilized to about 1,000 RU was used as ligand for the analyte binding of anti-FLT1 MAbs. An analyte range of 0–5 nM was used for kinetic experiments. A 5 min association step was used for each dilution followed by a 40 min dissociation. Chip surface was regenerated using pH 2.0 glycine between experiments.

ELISA

For the initial FLT1 blocking MAb screening, 96 well ELISA plates (44-2404-21, ThermoFisher Scientific) were incubated with mouse FLT1-FC chimeric protein with His-tag (471-F1-100, R&D Systems). Plates were washed with 0.05% Tween 20 in PBS, and blocked with 5% BSA (BP1600-1, Fisher Scientific) in PBS. After washing, diluted anti-FLT1 antibodies were incubated. After washing, recombinant mouse PlGF2 (465-PL-010/CF, R&D Systems) was incubated. After washing, biotin-conjugated anti-PlGF2 antibody (BAF465, R&D Systems) was added followed by a Streptavidin-HRP (R&D Systems, DY998). For a colorimetric detection, plates were developed with 3,3′,5,5′-Tetramethylbenzidine (TMB) Liquid Substrate (T0440, MilliporeSigma) and the reaction was stopped with 0.5M H_2SO_4. Specs were read at 450 nm on spectramax M5 plate reader (Molecular Devices). For VEGFA-FLT1 blocking assays, 96 wells ELISA plates were incubated with recombinant mouse VEGFA ($VEGF_{164}$) (493-MV-025/CF, R&D Systems,). After washing, anti-FLT1 antibodies were incubated with mouse

FLT1-FC chimeric protein with His-tag (471-F1-100, R&D Systems). After incubation the antibody-FLT1-FC complex was added to the VEGFA-coated plates. A biotin conjugated anti-His-tag antibody (NB100-63172, Bio-Connect) was added followed by a Streptavidin-HRP (DY998, R&D Systems). For a colorimetric detection, TMB was used as described above. For measurement of free sFlt1 and VEGFA in the serum. Animals were IV injected with 20 mg/kg body weight either isotype control IgG or the MAB0702 twice a week for 4 weeks beginning at 4 weeks of age. Blood was collected for biomarker analysis. Serum concentrations of sFLT1 and VEGFA were measured by ELISA kits following company recommended protocols (DY471 and DY493, R&D Systems). For a colorimetric detection, TMB was used as described above.

Statistics

Statistics and graphs were calculated using GraphPad 7.1 (Prism). Students t-test or ANOVA was used to compare two or more groups. Multiple comparison adjustment was performed with comparisons of 3 groups or more. * indicates $p<0.05$, ** indicates $p<0.01$, and *** indicates $p<0.001$.

Supporting information

S1 Fig. Confirmation of conditional deletion of *Flt1*. A. Immunostaining for FLT1 (green, arrows) and Laminin (red) shows effective deletion of FLT1 in TA muscle of $Flt1^{\Delta/\Delta}$ mice following tamoxifen (TMX) injection. DAPI staining (blue) is for all nuclei. Scale bars indicate 20 μm.
B. RT-qPCR shows deletion of the *Flt1* exon 3 in the TA muscle of $Flt1^{\Delta/\Delta}$ mice while exons 1 and 2 are retained.
C. $Flt1^{\Delta/\Delta}$ male mice show no difference in the body mass during the time course
D. $Flt1^{\Delta/\Delta}$ male mice show no difference in TA muscle mass compared to $Flt1^{+/+}$ male mice.
(PDF)

S2 Fig. Generation of *mdx*:$CAG^{CreERTM}$:$Flt1^{LoxP/LoxP}$ mice. A. *mdx*:$CAG^{CreERTM}$:$Flt1^{LoxP/LoxP}$ mice breed with *mdx*:$Flt1^{LoxP/LoxP}$ mice, and yield mice in expected ratios in a total of 92 mice genotyped. Chi-squared test shows no difference in expected.
B. Induction of $CreER^{TM}$ by TMX or 4-hydroxy-tamoxifen (4-OHT) shows that *Flt1* deletion in *mdx* mice prior to p21 results in partial or complete lethality in the *mdx*:$Flt1^{\Delta/\Delta}$ but not control $Flt1^{+/+}$ mice.
C. *mdx*:$Flt1^{\Delta/\Delta}$ mice show reduced male body mass but no difference in (D) muscle mass.
(PDF)

S3 Fig. Phenotyping of *mdx*:$Flt1^{\Delta/\Delta}$ mice. A. *mdx*:$Flt1^{\Delta/\Delta}$ mice show signs of premature aging such as white hair.
B. Representative image of type I slow MHC (green) and Laminin (red) in EDL and soleus muscle in *mdx*:$Flt1^{+/+}$ and *mdx*:$Flt1^{\Delta/\Delta}$ mice. Scale bars indicate 200 μm.
C. Type I slow MHC+ fibers are increased in the *mdx*:$Flt1^{\Delta/\Delta}$ mice in both EDL and Soleus muscle.
D. Representative image of eMHC (green) and Laminin (red) in EDL and soleus muscle in *mdx*:$Flt1^{+/+}$ and *mdx*:$Flt1^{\Delta/\Delta}$ mice. Scale bars indicate 200 μm.
D. eMHC staining shows decreased fiber stability in muscle fibers in the soleus but not the EDL muscle in the *mdx*:$Flt1^{\Delta/\Delta}$ mice.
(PDF)

S4 Fig. Validation of *Cdh5*^{CreERT2} and *mdx:Cdh5-Flt1*$^{\Delta/\Delta}$ mice. A. Experimental scheme for assessing angiogenic response from conditional *Flt1* deletion.
B. *Cdh5*^{CreERT2}:*Rosa26R*^{mTmG} mice reveal that *Cdh5*^{CreERT2} efficiently induced mGFP expression in the capillaries (green) labeled with lectin (purple), but not in other cell types including muscle fibers (red). Scale bars indicate 20 μm.
C. *Cdh5*^{CreERT2}:*Rosa26R*^{mTmG} mice show efficient mGFP labeling of lectin+ and CD31+ endothelial cells. Histogram indicates that more than 90% of the cells are CD31+mGFP+ or lectin +mGFP+.
D.E. Body mass and TA muscle mass are unchanged in *Cdh5-Flt1*$^{+/+}$ and *Cdh5-Flt1*$^{\Delta/\Delta}$ mice.
(PDF)

S5 Fig. Validation of *mdx:Cdh5-Flt1*$^{\Delta/\Delta}$ mice. A. B. Body mass and TA muscle mass are unchanged in *mdx*:*Cdh5-Flt1*$^{+/+}$*and mdx*:*Cdh5-Flt1*$^{\Delta/\Delta}$ mice.
C. D. Body mass is unchanged in male or female *mdx*:*Cdh5-Flt1*$^{+/+}$and *mdx*:*Cdh5-Flt1*$^{\Delta/\Delta}$ mice during the time course.
(PDF)

S6 Fig. Efficacy of anti-FLT1 peptide following intramuscular injection in the TA muscle of *mdx* mice. A. Experimental scheme for proof of principle study of *mdx* mice with intramuscular injection of anti-FLT1 peptide.
B. Representative images of CD31 (top) and EBD staining (bottom) of TA muscle injected with anti-FLT1 peptide. Scale bars indicate 50 μm.
C. Neonatal intramuscular injection of anti-FLT1 peptide increases capillary density in the TA muscle of the *mdx* mice.
D. Neonatal intramuscular injection of anti-FLT1 peptide decreases EBD+ area in the TA muscle of the *mdx* mice.
E. F. Systemic anti-FLT1 peptide injection does not change body mass in the male or female *mdx* mice at low or high dose.
(PDF)

S7 Fig. Systemic anti-FLT1 peptide injection improves muscle pathology without increase in leukocytes or neurologic phenotype in *mdx* mice. A. Representative images of HE staining, eMHC staining of diaphragm and Giemsa staining of blood smears in *mdx* mice treated with anti-FLT1 peptide. Allows indicate myeloid cells and lymphocytes. Scale bars indicate 100 μm.
B. Diaphragm muscle fiber turnover is reduced in *mdx* mice treated with anti-FLT1 peptide as evaluated by centrally located nuclei (CLN).
C. eMHC staining shows increased fiber stability in muscle fibers in the diaphragm of *mdx* mice treated with anti-FLT1 peptide.
D. No difference in motor coordination or balance on the Rotarod was observed between the groups.
(PDF)

S8 Fig. Systemic PEG-anti-FLT1 peptide injection does not improve skeletal muscle pathology in *mdx* mice. A. Experimental scheme for systemic treatment of *mdx* mice with IP injection of PEG-anti-FLT1 peptide.
B. Systemic PEG-anti-FLT1 peptide injection does not change body mass in the male *mdx* mice at low or high dose.
C. Systemic PEG-anti-FLT1 peptide injection does not increase capillary density in the *mdx* mice at low or high dose.
D. Systemic PEG-anti-FLT1 peptide injection does not decrease EBD in the *mdx* mice at low

or high dose.
E. Systemic PEG-anti-FLT1 peptide injection does not improve grip strength in the *mdx* mice at low or high dose.
(PDF)

S9 Fig. Screening for commercially available antibodies against FLT1 and phenotyping of *mdx* mice treated with MAB0702. A. Commercially available MAbs for anti-FLT1 screened for blocking activity against PlGF using ELISA. AF471 polyclonal anti-FLT1 antibody was used as a positive control. AP, Angio-Proteomie; SC, Santa Cruz Biotechnology.
B. Two selected MAbs screened for blocking activity against VEGFA using ELISA. AF471 polyclonal anti-FLT1 antibody was used as a positive control. AP, Angio-Proteomie.
C. Serum free sFLT1 is decreased in mice injected with MAB0702 compared to isotype control.
D. Serum free VEGFA is increased following MAB0702 treatment.
E. F. Systemic anti-FLT1 antibody injection does not change body mass in the male or female *mdx* mice.
(PDF)

S1 Table. Summary of mice used for this paper.
(PDF)

S2 Table. Biacore analysis for affinity of monoclonal antibodies against FLT1.
(PDF)

S3 Table. DNA primer sequences.
(PDF)

Acknowledgments

We thank Dr. Yoshiaki Kubota for kindly providing $Cdh5^{CreERT2}$ mice. We would like to thank Jake Trask for a critical reading.

Author Contributions

Conceptualization: Atsushi Asakura.

Data curation: Mayank Verma, Yuko Shimizu-Motohashi, Yoko Asakura, James P. Ennen, Atsushi Asakura.

Formal analysis: Mayank Verma, Yuko Shimizu-Motohashi, Yoko Asakura, Jennifer Bosco, Zhiwei Zhou, Dennis Keefe, Atsushi Asakura.

Funding acquisition: Mayank Verma, Atsushi Asakura.

Investigation: Mayank Verma, Yuko Shimizu-Motohashi, Yoko Asakura, James P. Ennen, Jennifer Bosco, Zhiwei Zhou, Atsushi Asakura.

Methodology: Mayank Verma.

Project administration: Serene Josiah, Dennis Keefe, Atsushi Asakura.

Resources: Guo-Hua Fong, Serene Josiah, Dennis Keefe, Atsushi Asakura.

Supervision: Atsushi Asakura.

Validation: Atsushi Asakura.

Writing – original draft: Mayank Verma.

Writing – review & editing: Atsushi Asakura.

References

1. Im W. B., Phelps S. F., Copen E. H., Adams E. G., Slightom J. L., Chamberlain J. S. Differential expression of dystrophin isoforms in strains of mdx mice with different mutations. Hum Mol Genet. 1996; 5 (8):1149–53. https://doi.org/10.1093/hmg/5.8.1149 PMID: 8842734.
2. Miyatake M, Miike T, Zhao J, Yoshioka K, Uchino M, Usuku G. Possible systemic smooth muscle layer dysfunction due to a deficiency of dystrophin in Duchenne muscular dystrophy. J Neurol Sci. 1989; 93 (1):11–7. https://doi.org/10.1016/0022-510x(89)90157-3 PMID: 2681539
3. Loufrani L, Matrougui K, Gorny D, Duriez M, Blanc I, Levy BI, et al. Flow (shear stress)-induced endothelium-dependent dilation is altered in mice lacking the gene encoding for dystrophin. Circulation. 2001; 103:864–70. https://doi.org/10.1161/01.cir.103.6.864 PMID: 11171796
4. Ito K, Kimura S, Ozasa S, Matsukura M, Ikezawa M, Yoshioka K, et al. Smooth muscle-specific dystrophin expression improves aberrant vasoregulation in mdx mice. Hum Mol Genet. 2006; 15(14):2266–75. https://doi.org/10.1093/hmg/ddl151 PMID: 16777842
5. Coral-Vazquez R, Cohn RD, Moore SA, Hill JA, Weiss RM, Davisson RL, et al. Disruption of the sarcoglycan-sarcospan complex in vascular smooth muscle: a novel mechanism for cardiomyopathy and muscular dystrophy. Cell. 1999; 98(4):465–74. https://doi.org/10.1016/s0092-8674(00)81975-3 PMID: 10481911
6. Lai Y, Thomas GD, Yue Y, Yang HT, Li D, Long C, et al. Dystrophins carrying spectrin-like repeats 16 and 17 anchor nNOS to the sarcolemma and enhance exercise performance in a mouse model of muscular. J Clin Invest. 2009; 119(3):624–35. https://doi.org/10.1172/JCI36612 PMID: 19229108
7. Asai A, Sahani N, Kaneki M, Ouchi Y, Martyn JA, Yasuhara SE. Primary role of functional ischemia, quantitative evidence for the two-hit mechanism, and phosphodiesterase-5 inhibitor therapy in mouse muscular dystrophy. PloS one. 2007; 2(8):e806. Epub 2007/08/30. https://doi.org/10.1371/journal.pone.0000806 PMID: 17726536; PubMed Central PMCID: PMC1950086.
8. Adamo CM, Dai DF, Percival JM, Minami E, Willis MS, Patrucco E, et al. Sildenafil reverses cardiac dysfunction in the mdx mouse model of Duchenne muscular dystrophy. Proc Natl Acad Sci U S A. 2010; 107:19079–83. https://doi.org/10.1073/pnas.1013077107 PMID: 20956307
9. Martin EA, Barresi R, Byrne BJ, Tsimerinov EI, Scott BL, Walker AE, et al. Tadalafil Alleviates Muscle Ischemia in Patients with Becker Muscular Dystrophy. Sci Transl Med. 2012; 4(162):162ra55. https://doi.org/10.1126/scitranslmed.3004327 PMID: 23197572.
10. Nelson MD, Rader F, Tang X, Tavyev J, Nelson SF, Miceli MC, et al. PDE5 inhibition alleviates functional muscle ischemia in boys with Duchenne muscular dystrophy. Neurology. 2014:1–7. https://doi.org/10.1212/WNL.0000000000000498 PMID: 24808022.
11. Matsakas A, Yadav V, Lorca S, Narkar V. Muscle ERRγ mitigates Duchenne muscular dystrophy via metabolic and angiogenic reprogramming. FASEB J. 2013; 27(10):4004–16. https://doi.org/10.1096/fj.13-228296 PMID: 23781095.
12. Latroche C, Matot B, Martins-Bach A, Briand D, Chazaud B, Wary C, et al. Structural and Functional Alterations of Skeletal Muscle Microvasculature in Dystrophin-Deficient mdx Mice. Am J Pathol. 2015:1–13. https://doi.org/10.1016/j.ajpath.2015.05.009 PMID: 26193666
13. Shibuya M. and dual function of vascular endothelial growth factor receptor-1 (Flt-1). Int J Biochem Cell Biol. 2001; 33(4):409–20. https://doi.org/10.1016/s1357-2725(01)00026-7 PMID: 11312109.
14. Kendall RL, Thomas KA. Inhibition of vascular endothelial cell growth factor activity by an endogenously encoded soluble receptor. Proc Natl Acad Sci U S A. 1993; 90(22):10705–9. https://doi.org/10.1073/pnas.90.22.10705 PMID: 8248162; PubMed Central PMCID: PMC47846.
15. Verma M, Asakura Y, Hirai H, Watanabe S, Tastad C, Fong GH, et al. Flt-1 haploinsufficiency ameliorates muscular dystrophy phenotype by developmentally increased vasculature in mdx mice. Hum Mol Genet. 2010; 19(21):4145–59. https://doi.org/10.1093/hmg/ddq334 PMID: 20705734.
16. Sawano a, Iwai S, Sakurai Y, Ito M, Shitara K, Nakahata T, et al. Flt-1, vascular endothelial growth factor receptor 1, is a novel cell surface marker for the lineage of monocyte-macrophages in humans. Blood. 2001; 97:785–91. https://doi.org/10.1182/blood.v97.3.785 PMID: 11157498
17. Poesen K, Lambrechts D, Van Damme P, Dhondt J, Bender F, Frank N, et al. Novel role for vascular endothelial growth factor (VEGF) receptor-1 and its ligand VEGF-B in motor neuron degeneration. J Neurosci. 2008; 28(42):10451–9. https://doi.org/10.1523/JNEUROSCI.1092-08.2008 PMID: 18923022; PubMed Central PMCID: PMC6671326.

18. Fong GH, Zhang L, Bryce DM, Peng J. Increased hemangioblast commitment, not vascular disorganization, is the primary defect in flt-1 knock-out mice. Development. 1999; 126(13):3015–25. PMID: 10357944

19. Hayashi S, McMahon AP. Efficient recombination in diverse tissues by a tamoxifen-inducible form of Cre: a tool for temporally regulated gene activation/inactivation in the mouse. Dev Biol. 2002; 244:305–18. https://doi.org/10.1006/dbio.2002.0597 PMID: 11944939.

20. Ho VC, Duan LJ, Cronin C, Liang BT, Fong GH. Elevated vascular endothelial growth factor receptor-2 abundance contributes to increased angiogenesis in vascular endothelial growth factor receptor-1-deficient mice. Circulation. 2012; 126(6):741–52. https://doi.org/10.1161/CIRCULATIONAHA.112.091603 PMID: 22753193.

21. Seki T, Hosaka K, Fischer C, Lim S, Andersson P, Abe M, et al. Ablation of endothelial VEGFR1 improves metabolic dysfunction by inducing adipose tissue browning. J Exp Med. 2018; 215(2):611–26. https://doi.org/10.1084/jem.20171012 PMID: 29305395; PubMed Central PMCID: PMC5789413.

22. Waters RE, Rotevatn S, Li P, Annex BH, Yan Z. Voluntary running induces fiber type-specific angiogenesis in mouse skeletal muscle. Am J Physiol Cell Physiol. 2004; 287(5):C1342–8. https://doi.org/10.1152/ajpcell.00247.2004 PMID: 15253894

23. Webster C, Silberstein L, Hays AP, Blau HM. Fast muscle fibers are preferentially affected in Duchenne muscular dystrophy. Cell. 1988; 52(4):503–13. Epub 1988/02/26. https://doi.org/10.1016/0092-8674(88)90463-1 PMID: 3342447.

24. Rafael JA, Townsend ER, Squire SE, Potter AC, Chamberlain JS, Davies KE. Dystrophin and utrophin influence fiber type composition and post-synaptic membrane structure. Hum Mol Genet. 2000; 9(9):1357–67. https://doi.org/10.1093/hmg/9.9.1357 PMID: 10814717.

25. Call JA, Warren GL, Verma M, Lowe DA. Acute failure of action potential conduction in mdx muscle reveals new mechanism of contraction-induced force loss. J Physiol. 2013; 591(15):3765–76. https://doi.org/10.1113/jphysiol.2013.254656 PMID: 23753524.

26. Robciuc MR, Kivela R, Williams IM, de Boer JF, van Dijk TH, Elamaa H, et al. VEGFB/VEGFR1-Induced Expansion of Adipose Vasculature Counteracts Obesity and Related Metabolic Complications. Cell Metab. 2016; 23(4):712–24. https://doi.org/10.1016/j.cmet.2016.03.004 PMID: 27076080; PubMed Central PMCID: PMC5898626.

27. Okabe K, Kobayashi S, Yamada T, Kurihara T, Tai-nagara I. Neurons Limit Angiogenesis by Titrating VEGF in Retina. Cell. 2014; 159:584–96. https://doi.org/10.1016/j.cell.2014.09.025 PMID: 25417109

28. Goel AJ, Rieder MK, Arnold HH, Radice GL, Krauss RS. Niche Cadherins Control the Quiescence-to-Activation Transition in Muscle Stem Cells. Cell Rep. 2017; 21(8):2236–50. https://doi.org/10.1016/j.celrep.2017.10.102 PMID: 29166613; PubMed Central PMCID: PMC5702939.

29. Kong J-S, Yoo S-A, Kang J-H, Ko W, Jeon S, Chae C-B, et al. Suppression of neovascularization and experimental arthritis by D-form of anti-flt-1 peptide conjugated with mini-PEG(™). Angiogenesis. 2011; 14:431–42. https://doi.org/10.1007/s10456-011-9226-0 PMID: 21751011.

30. Liston DR, Davis M. Clinically Relevant Concentrations of Anticancer Drugs: A Guide for Nonclinical Studies. Clin Cancer Res. 2017; 23(14):3489–98. https://doi.org/10.1158/1078-0432.CCR-16-3083 PMID: 28364015; PubMed Central PMCID: PMC5511563.

31. Christinger HW, Fuh G, de Vos AM, Wiesmann C. The crystal structure of placental growth factor in complex with domain 2 of vascular endothelial growth factor receptor-1. J Biol Chem. 2004; 279(11):10382–8. https://doi.org/10.1074/jbc.M313237200 PMID: 14684734.

32. Springer ML, Ozawa CR, Banfi A, Kraft PE, Ip TK, Brazelton TR, et al. Localized arteriole formation directly adjacent to the site of VEGF-induced angiogenesis in muscle. Mol Ther. 2003; 7(4):441–9. https://doi.org/10.1016/s1525-0016(03)00010-8 PMID: 12727106

33. Frank RT, Aboody KS, Najbauer J. Strategies for enhancing antibody delivery to the brain. Biochim Biophys Acta. 2011; 1816(2):191–8. https://doi.org/10.1016/j.bbcan.2011.07.002 PMID: 21767610.

34. Lalatsa A, Schatzlein AG, Uchegbu IF. Strategies to deliver peptide drugs to the brain. Mol Pharm. 2014; 11(4):1081–93. https://doi.org/10.1021/mp400680d PMID: 24601686.

35. Miquerol L, Langille BL, Nagy A. Embryonic development is disrupted by modest increases in vascular endothelial growth factor gene expression. Development. 2000; 127(18):3941–6. PMID: 10952892.

36. Gabhann FM, Ji JW, Popel AS. Computational model of vascular endothelial growth factor spatial distribution in muscle and pro-angiogenic cell therapy. PLoS Comput Biol. 2006; 2:1107–20. https://doi.org/10.1371/journal.pcbi.0020127 PMID: 17002494.

37. Logsdon EA, Finley SD, Popel AS, F. MF. A systems biology view of blood vessel growth and remodelling. J Cell Mol Med. 2014; 18:1491–508. https://doi.org/10.1111/jcmm.12164 PMID: 24237862.

38. Verma M, Asakura Y, Murakonda BSR, Pengo T, Latroche C, Chazaud B, et al. Muscle Satellite Cell Cross-Talk with a Vascular Niche Maintains Quiescence via VEGF and Notch Signaling. Cell Stem Cell.

2018; 23(4):530–43 e9. https://doi.org/10.1016/j.stem.2018.09.007 PMID: 30290177; PubMed Central PMCID: PMC6178221.

39. Koch S, Tugues S, Li X, Gualandi L, Claesson-Welsh L. Signal transduction by vascular endothelial growth factor receptors. Biochem J. 2011; 437:169–83. https://doi.org/10.1042/BJ20110301 PMID: 21711246.

40. Dewerchin M, Carmeliet P. PlGF: a multitasking cytokine with disease-restricted activity. Cold Spring Harb Perspect Med. 2012; 2(8). https://doi.org/10.1101/cshperspect.a011056 PMID: 22908198; PubMed Central PMCID: PMC3405829.

41. Olofsson B, Pajusola K, Kaipainen A, von Euler G, Joukov V, Saksela O, et al. Vascular endothelial growth factor B, a novel growth factor for endothelial cells. Proc Natl Acad Sci U S A. 1996; 93(6):2576–81. https://doi.org/10.1073/pnas.93.6.2576 PMID: 8637916; PubMed Central PMCID: PMC39839.

42. Hagberg CE, Mehlem A, Falkevall A, Muhl L, Fam BC, Ortsater H, et al. Targeting VEGF-B as a novel treatment for insulin resistance and type 2 diabetes. Nature. 2012; 490(7420):426–30. https://doi.org/10.1038/nature11464 PMID: 23023133.

43. Li X, Tjwa M, Van Hove I, Enholm B, Neven E, Paavonen K, et al. Reevaluation of the role of VEGF-B suggests a restricted role in the revascularization of the ischemic myocardium. Arterioscler Thromb Vasc Biol. 2008; 28(9):1614–20. https://doi.org/10.1161/ATVBAHA.107.158725 PMID: 18511699; PubMed Central PMCID: PMC2753879.

44. Messina S, Mazzeo A, Bitto A, Aguennouz M, Migliorato A, De Pasquale MG, et al. VEGF overexpression via adeno-associated virus gene transfer promotes skeletal muscle regeneration and enhances muscle function in mdx mice. FASEB J. 2007; 21(13):3737–46. https://doi.org/10.1096/fj.07-8459com PMID: 17575261.

45. Deasy BM, Feduska JM, Payne TR, Li Y, Ambrosio F, Huard J. Effect of VEGF on the regenerative capacity of muscle stem cells in dystrophic skeletal muscle. Mol Ther. 2009; 17(10):1788–98. https://doi.org/10.1038/mt.2009.136 PMID: 19603004; PubMed Central PMCID: PMC2835014.

46. Gianni-Barrera R, Trani M, Fontanellaz C, Heberer M, Djonov V, Hlushchuk R, et al. VEGF over-expression in skeletal muscle induces angiogenesis by intussusception rather than sprouting. Angiogenesis. 2013; 16:123–36. https://doi.org/10.1007/s10456-012-9304-y PMID: 22961440.

47. Song X, Zhang Y, Hou Z, Wu H, Lu S, Tang J, et al. Adeno-associated virus serotype 9 mediated vascular endothelial growth factor gene overexpression in mdx mice. Exp Ther Med. 2018; 15(2):1825–30. https://doi.org/10.3892/etm.2017.5610 PMID: 29434771; PubMed Central PMCID: PMC5776553.

48. Latroche C, Weiss-Gayet M, Muller L, Gitiaux C, Leblanc P, Liot S, et al. Coupling between Myogenesis and Angiogenesis during Skeletal Muscle Regeneration Is Stimulated by Restorative Macrophages. Stem Cell Reports. 2017; 9(6):2018–33. https://doi.org/10.1016/j.stemcr.2017.10.027 PMID: 29198825; PubMed Central PMCID: PMC5785732.

49. Christov C, Chretien F, Abou-Khalil R, Bassez G, Vallet G, Authier FJ, et al. Muscle satellite cells and endothelial cells: close neighbors and privileged partners. Mol Biol Cell. 2007; 18(4):1397–409. https://doi.org/10.1091/mbc.E06-08-0693 PMID: 17287398

50. Saitoh M, Ishida J, Ebner N, Anker SD, von Haehling S. Myostatin inhibitors as pharmacological treatment for muscle wasting and muscular dystrophy. JCSM Clin Reports 2017; 2(1):e00037.

51. Wallace B, Peisl A, Seedorf G, Nowlin T, Kim C, Bosco J, et al. Anti-sFlt-1 Therapy Preserves Lung Alveolar and Vascular Growth in Antenatal Models of Bronchopulmonary Dysplasia. Am J Respir Crit Care Med. 2018; 197(6):776–87. https://doi.org/10.1164/rccm.201707-1371OC PMID: 29268623; PubMed Central PMCID: PMC5855071.

52. Danko I, Chapman V, Wolff JA. The frequency of revertants in mdx mouse genetic models for Duchenne muscular dystrophy. Pediatr Res. 1992; 32(1):128–31. https://doi.org/10.1203/00006450-199207000-00025 PMID: 1635838

53. Muzumdar MD, Tasic B, Miyamichi K, Li L, Luo L. A global double-fluorescent Cre reporter mouse. Genesis. 2007; 45(9):593–605. https://doi.org/10.1002/dvg.20335 PMID: 17868096.

54. Bae DG, Kim TD, Li G, Yoon WH, Chae CB. Anti-flt1 peptide, a vascular endothelial growth factor receptor 1-specific hexapeptide, inhibits tumor growth and metastasis. Clin Cancer Res. 2005; 11:2651–61. https://doi.org/10.1158/1078-0432.CCR-04-1564 PMID: 15814646

55. Aartsma-Rus A, van Putten M. Assessing functional performance in the mdx mouse model. J Vis Exp. 2014;(85). https://doi.org/10.3791/51303 PMID: 24747372; PubMed Central PMCID: PMC4158772.

56. Fukada S, Morikawa D, Yamamoto Y, Yoshida T, Sumie N, Yamaguchi M, et al. Genetic background affects properties of satellite cells and mdx phenotypes. Am J Pathol. 2010; 176:2414–24. https://doi.org/10.2353/ajpath.2010.090887 PMID: 20304955.

57. Jin Q, Qiao C, Li J, Xiao B, Li J, Xiao X. A GDF11/myostatin inhibitor, GDF11 propeptide-Fc, increases skeletal muscle mass and improves muscle strength in dystrophic mdx mice. Skelet Muscle. 2019; 9

(1):16. https://doi.org/10.1186/s13395-019-0197-y PMID: 31133057; PubMed Central PMCID: PMC6537384.

58. Schindelin J, Arganda-Carreras I, Frise E, Kaynig V, Longair M, Pietzsch T, et al. Fiji: an open-source platform for biological-image analysis. Nat Methods. 2012; 9:676–82. https://doi.org/10.1038/nmeth.2019 PMID: 22743772.